

Electronic Supplementary Information (ESI) for  
Tungsten-based Solar Absorber with a Strip-Combined Starfish Structure  
Physical Chemistry Chemical Physics, 2025

## S1. Pre-optimization results

To provide a direct comparison with the optimized structures presented in the main text, we also evaluated the optical performance of the corresponding unoptimized counterparts. The results are summarized in Figures S1–S4:

- Figure S1 presents the angular dependence of  $\alpha_{\text{total}}$  for the baseline square block structure ( $0.25 \times 0.25 \times 0.15 \mu\text{m}$ ). The unoptimized structure shows only moderate angular stability compared with the optimized design in Figure 10 of the main text.
- Figure S2 shows the spectral response of the unoptimized counterpart of the freehand drawing structure, which achieves  $\alpha_{\text{total}} = 0.905$ . This value is lower than that of the optimized freehand design (Figure 11 in the main text), indicating the effectiveness of the optimization.
- Figure S3 gives the variation of  $\alpha_{\text{total}}$  with edge angle for the unoptimized square block structure, corresponding to Figure 12 in the main text. In contrast to the optimized case, the absorptance decreases as the edge angle increases, highlighting the importance of structural tailoring.
- Figure S4 provides the spectral absorptance and thermal emission of the unoptimized structure, corresponding to Figure 13 in the main text. Compared with the optimized design, the unoptimized case exhibits weaker suppression of mid-infrared emission, confirming the benefit of optimization for selective thermal management.

Overall, these results demonstrate that the optimized structures consistently outperform their unoptimized counterparts in terms of both broadband solar absorption and thermal emission control, underscoring the necessity of the optimization process.

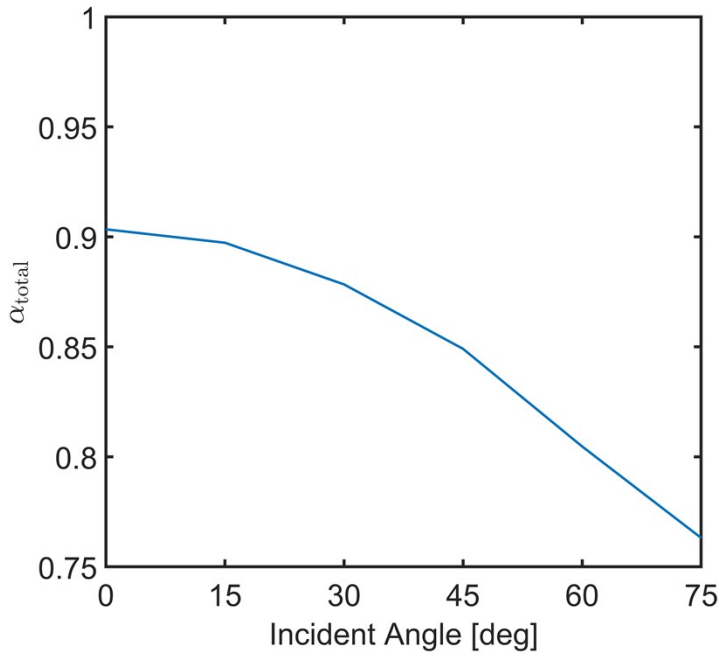


Figure S1. Simulated angular dependence of the total absorptance ( $\alpha_{\text{total}}$ ) for the unoptimized baseline structure. The absorptance decreases gradually with increasing incident angle from  $0^\circ$  to  $75^\circ$ .

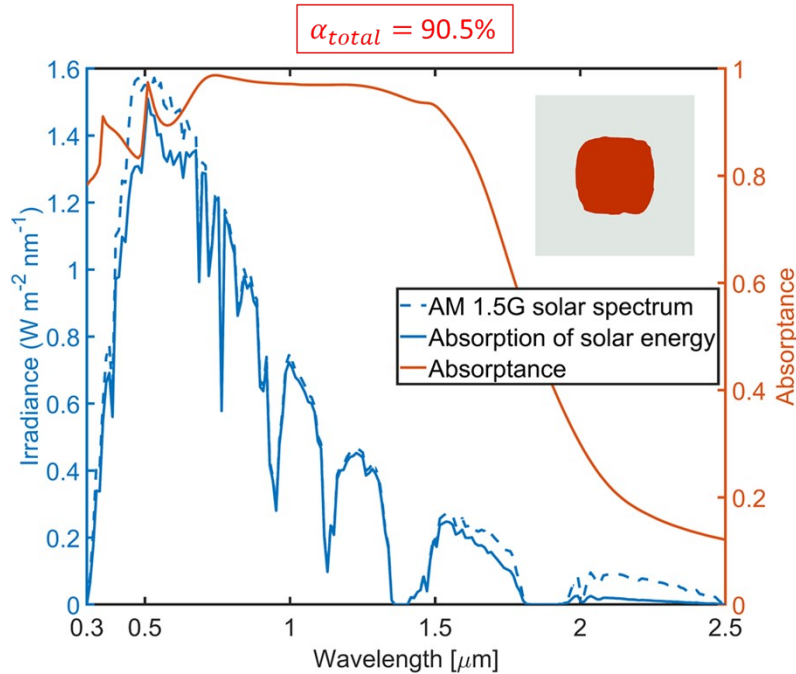


Figure S2. Spectral response of the unoptimized counterpart of the freehand drawing structure (square pillar,  $0.25 \times 0.25 \times 0.15 \mu\text{m}$ ; inset). The orange curve shows the absorptance  $A(\lambda)$  (right axis). The dashed blue curve is the AM1.5G solar spectrum and the solid blue curve is the absorbed solar power density  $A(\lambda) \times \text{AM1.5G}(\lambda)$  (left axis). The AM1.5G-weighted total absorptance is  $\alpha_{\text{total}} = 0.905$  (90.5%).

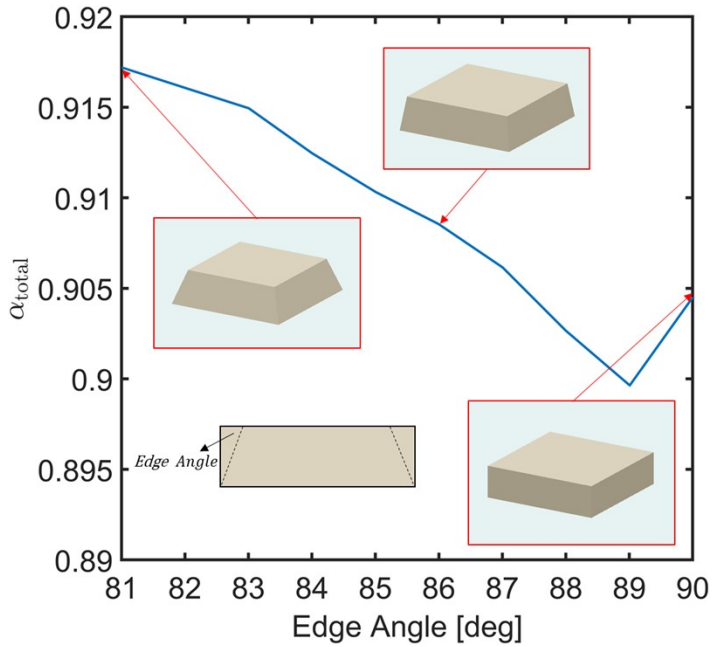


Figure S3. Total absorptance ( $\alpha_{\text{total}}$ ) of the unoptimized square block structure as a function of edge angle (81–90°). The insets illustrate representative geometries at selected edge angles. This figure corresponds to the unoptimized counterpart of Figure 12 in the main text.

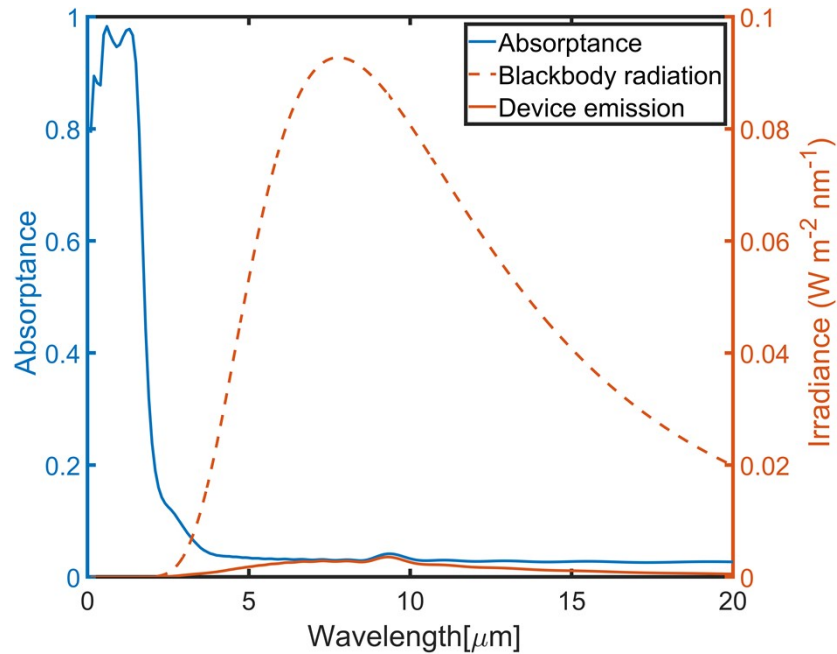


Figure S4. Spectral absorptance and corresponding thermal emission of the unoptimized structure. The blue curve shows the absorptance  $A(\lambda)$  (left axis). The dashed brown curve indicates the blackbody radiation spectrum at 100 °C, while the solid brown curve represents the calculated emission of the device (right axis). This figure corresponds to the unoptimized counterpart of Figure 13 in the main text.

## S2. FDTD simulation and PSO optimization

The optical response of the structures was calculated using the finite-difference time-domain (FDTD) method implemented in Lumerical FDTD Solutions (Ansys Inc.). The minimum mesh step was set to 2.5 nm to resolve subwavelength features, and the time step was determined using a stability factor of 0.99 to ensure numerical stability. Periodic boundary conditions were applied in the x and y directions to represent an infinite array, while perfectly matched layers (PMLs) were used in the z direction to suppress non-physical reflections. The PML thickness was set to 8 layers, with a standard stretched-coordinate profile ( $\kappa = 2$ ,  $\sigma = 1$ , polynomial order = 3). These settings provided a balance between computational efficiency and spectral convergence.

For geometry optimization, a particle swarm optimization (PSO) algorithm was coupled with the FDTD solver to maximize the total solar absorptance ( $\alpha_{\text{total}}$ ) in the 0.3–2.5  $\mu\text{m}$  range. The setup followed the Optimization utility provided in Lumerical [1], where  $\alpha_{\text{total}}$  was defined as a single scalar figure of merit (FOM). In our implementation, the swarm size was set to 5 with a fixed budget of 1000 iterations. The convergence tolerance was set to zero (i.e., early stopping was disabled), so the optimizer ran for all 1000 iterations; the solution stabilized after the first several generations with no further improvement.

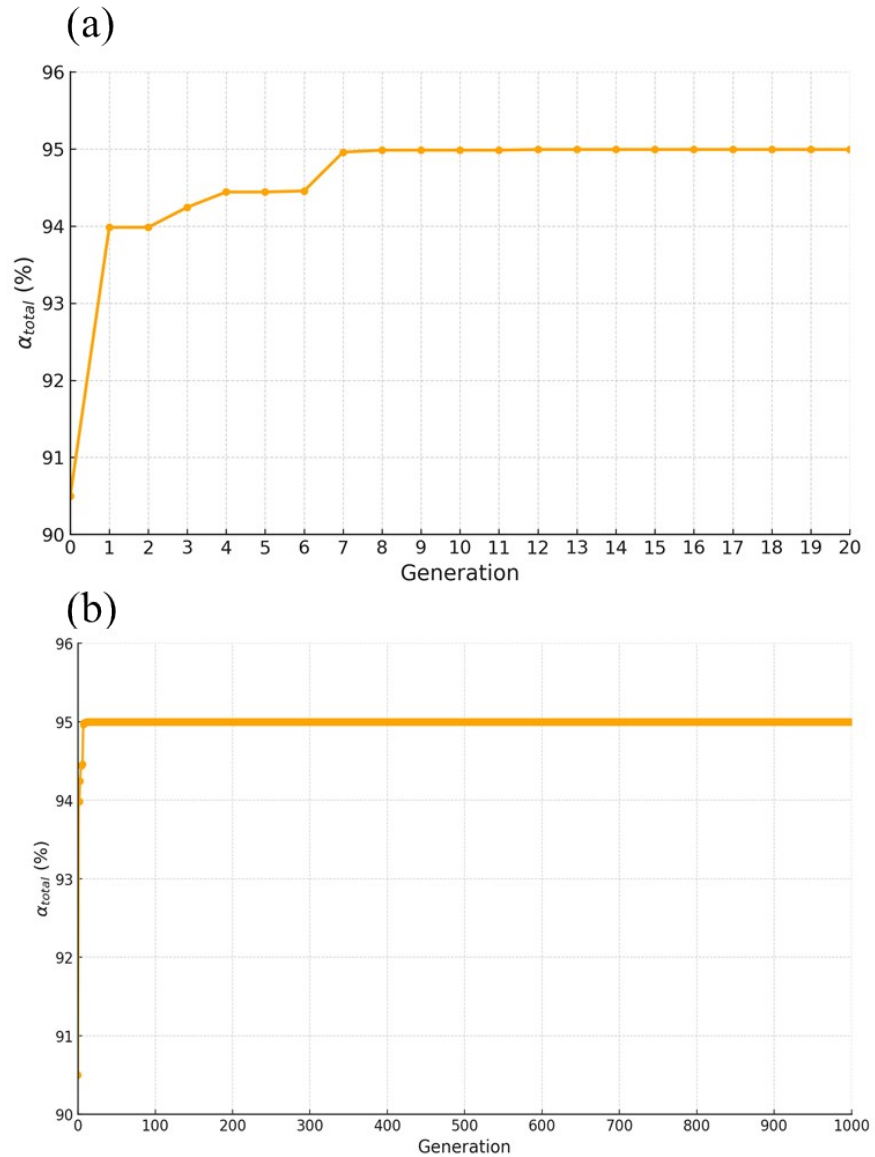


Figure S5. Convergence behavior of the particle swarm optimization (PSO). (a) The optimization rapidly converges within the first  $\sim 10$  generations, starting from an initial  $\alpha_{total} = 90.5\%$  and reaching a stable maximum of  $95.0\%$ . (b) Extended run up to 1000 generations confirms that the solution remains stable without further improvement, indicating robust convergence of the PSO process.

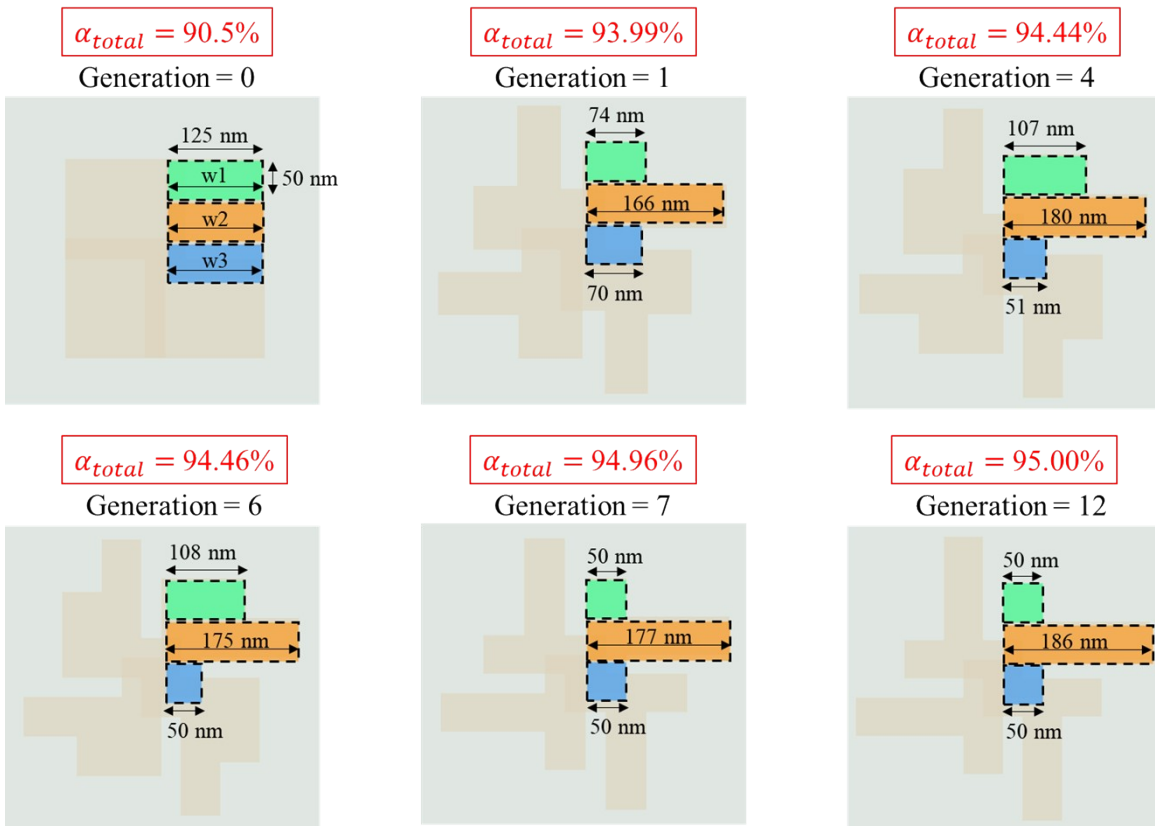


Figure S6. Structural evolution of the strip-combined absorber during PSO optimization. The figure shows selected generations (generation = 0, 1, 4, 6, 7, and 12) together with their corresponding total solar absorptance values  $\alpha_{total}$ . The dimensions of the three strip-like elements (w1, w2, w3) are labeled in each panel. The results illustrate how the initially symmetric square-like configuration ( $\alpha_{total} = 90.5\%$ ) progressively evolves toward an optimized structure with elongated central strip, leading to a higher absorptance of 95.0%.

## References for Supporting Information

[1] Lumerical Optimization Utility, Ansys Inc. Available at: <https://optics.ansys.com/hc/en-us/articles/360034922953-Optimization-utility>